Title

Estimation of fractional myocardial blood volume and water exchange using ferumoxytol-enhanced magnetic resonance imaging.

Journal

Journal of magnetic resonance imaging : JMRI, 53(6)

ISSN

1053-1807

Authors

Colbert, Caroline M
Thomas, Michael A
Yan, Ran
et al.

Publication Date

2021-06-01

DOI

10.1002/jmri.27494

Peer reviewed

HHS Public Access

Author manuscript

J Magn Reson Imaging. Author manuscript; available in PMC 2022 June 01.

Published in final edited form as:

J Magn Reson Imaging. 2021 June ; 53(6): 1699–1709. doi:10.1002/jmri.27494.

Estimation of fractional myocardial blood volume and water exchange using ferumoxytol-enhanced MRI

Caroline M. Colbert, BS[1], **Michael A. Thomas, MD**[2], **Ran Yan, BS**[3], **Aleksandra Radjenovic, PhD**[4], **J. Paul Finn, MD**[1,5], **Peng Hu, PhD**[1,3,5], **Kim-Lien Nguyen, MD**[1,2,5]

[1]Physics and Biology in Medicine Graduate Program, David Geffen School of Medicine at UCLA

[2]Division of Cardiology, David Geffen School of Medicine at UCLA and VA Greater Los Angeles Healthcare System

[3]Bioengineering Graduate Program, Henry Samueli School of Engineering and Applied Science at UCLA

[4]Institute of Cardiovascular & Medical Sciences, College of Medical, Veterinary and Life Sciences, University of Glasgow, UK

[5]Diagnostic Cardiovascular Imaging Laboratory, Department of Radiological Sciences, David Geffen School of Medicine at UCLA

Abstract

BACKGROUND: Fractional myocardial blood volume (fMBV) estimated using ferumoxytol-enhanced MRI (FE-MRI) has the potential to capture a hemodynamic response to myocardial hypoperfusion during contrast steady state without reliance on gadolinium chelates. Ferumoxytol has a long intravascular half-life and its use for steady-state MRI is off-label.

PURPOSE: To optimize and evaluate a two-compartment model for estimation of fMBV based on FE-MRI.

STUDY TYPE: Prospective

ANIMAL MODEL: Nine healthy swine; one swine with artificially-induced single-vessel coronary stenosis.

FIELD STRENGTH/SEQUENCE: 3.0T clinical magnet using the 5(3)3(3)3 Modified Look-Locker Inversion Recovery (MOLLI) sequence.

ASSESSMENT: Myocardial longitudinal spin-lattice relaxation rate (R1) was measured using the MOLLI sequence before and at contrast steady state following seven ferumoxytol infusions (0.125 – 4.0 mg/kg). fMBV and water exchange were estimated using a two-compartment model. Model-fitted fMBV was compared to simple fast-exchange fMBV approximation and percent change in pre and post-ferumoxytol R1. Dose under-sampling schemes were investigated to reduce acquisition duration.

Address correspondence to: Kim-Lien Nguyen, MD, David Geffen School of Medicine at UCLA, VA Greater Los Angeles Healthcare System, 11301 Wilshire Blvd, MC 111E, Los Angeles, CA 90073, Phone: 310.592.0386, Fax: 310.268.3258, klnguyen@ucla.edu.

STATISTICAL TESTS: Variation in fMBV was assessed with a one-way analysis of variance (ANOVA). Fast-exchange fMBV and ferumoxytol dose under-sampling were evaluated using Bland-Altman analysis.

RESULTS: Healthy normal swine showed a mean mid-ventricular fMBV of 7.2 ± 1.4% and water exchange rate of 11.3 ± 5.1 s^{-1}. There was inter-subject variation in fMBV ($p < 0.05$) without segmental variation (p=0.387). fMBV derived from eight-dose and four-dose sampling schemes had no significant bias (mean difference =0.07, p=0.541, limits of agreement −1.04% [−1.45, −0.62%] to 1.18% [0.77, 1.59%]). Pixel-wise fMBV in one swine model with coronary artery stenosis showed elevated fMBV in ischemic segments (apical anterior: 11.90 ± 4.00%, apical septum: 16.10 ± 5.71%) relative to remote segments (apical inferior: 9.59 ± 3.35%, apical lateral: 9.38 ± 2.35%).

DATA CONCLUSION: A two-compartment model based on FE-MRI using the MOLLI sequence may enable estimation of fMBV in studies of ischemic heart disease.

Keywords

Ferumoxytol; compartment modeling; tissue blood volume; swine model; T1 mapping

INTRODUCTION

Estimation of fractional tissue blood volume using MRI remains an area of intense research because it allows for a comprehensive evaluation of tissue or organ perfusion when combined with assessment of tissue blood flow and oxygen extraction fraction. Current quantitative clinical MRI approaches to identify perfusion surrogates rely on dynamic gadolinium-enhanced MRI (1, 2). Several clinically-relevant models exist (3), but all are limited by the lack of a true intravascular agent that is available in the clinic. The use of fractional blood volume as an indicator of overall tissue perfusion has broad applications for vital organs such as the heart, brain, kidney, and liver, but is most actively used in tumor imaging and staging. In this study, we will focus on the fractional myocardial blood volume (fMBV), which provides additional insight into myocardial ischemia severity beyond that provided by myocardial blood flow (MBF) alone (4, 5).

Multi-compartmental modelling can be used to quantify fMBV from contrast-enhanced cardiac MRI (6, 7). Of these models, two-compartment strategies have been used to describe the effect of contrast agents and vascular water exchange on MR signal intensity in the myocardium (6). One major challenge for measurement of fMBV in 2-compartment models however, is the intravascular fidelity and corresponding kinetics of the contrast agent. Thus, exploiting contrast agents with true intravascular properties for fMBV studies is an obvious choice because they eliminate the need to model contrast leakage into the extravascular space (1, 2). One such agent is ferumoxytol (Feraheme, AMAG Pharmaceuticals, Waltham, MA). As an ultrasmall superparamagnetic iron-oxide nanoparticle (mean diameter 30 nm) (8), ferumoxytol is approved for the intravenous treatment of iron deficiency anemia and is the only intravascular agent clinically available for off-label use as an MRI contrast agent (9–14). Its long intravascular half-life (10-14 hours) and high R1 relaxivity (9.5 s^{-1} mM^{-1} at 3.0T in human plasma at 37°C) (15, 16) make ferumoxytol an ideal intravascular contrast

agent for estimating fMBV. The clinical availability and better safety profile of ferumoxytol (compared to gadolinium-based agents) in patients with renal impairment are also desirable characteristics. Ferumoxytol, however, is only marketed in the United State and is its diagnostic use is off label.

We hypothesized that ferumoxytol-enhanced (FE) T1 MRI using a multi-dose sampling scheme could be combined with a two-compartment model to quantify fMBV as a proxy for myocardial perfusion. Consequently, the aim of this study was to derive and test a two-compartment, water exchange model based on FE-MRI for fMBV quantification and to compare it to other proposed T1 MRI proxies of blood volume estimation. We also aimed to define an optimal ferumoxytol dosing and sampling scheme needed to quantify fMBV, and to show in a swine model with coronary stenosis that fMBV differentiates hypoperfused and perfused myocardium.

MATERIALS AND METHODS

Theory for fMBV and Multi-Compartmental Water Exchange Modelling

Estimation of fMBV requires consideration of both contrast agent distribution volume and water exchange. Both the transvascular water exchange and transcytolemmal water exchange may affect MRI contrast and the apparent concentration of the contrast agent in the imaging voxel of interest. Although ferumoxytol functions as a purely intravascular contrast agent (17), the iron core has superparamagnetic properties and interacts with water protons that diffuse freely between the intravascular and extravascular spaces. Therefore, the post-contrast MRI signal intensity within any imaging voxel depends on both fMBV and the rate of exchange of water protons between the intravascular and extravascular spaces.

Prior work in human and animal studies has demonstrated that water exchange is both subject- and tissue-specific (17–19). The dependence of signal intensity on the rate of water exchange can be illustrated by the limiting cases of slow-exchange and fast-exchange (Appendix 1). At either the slow- or fast-exchange limit, fMBV could be computed from a single native and a single post-ferumoxytol image. However, neither exchange limit accurately represents myocardial physiology. Oversimplification of a parameterized model can result in increased bias and variance, and either exchange limit model can significantly over- or underestimate fMBV, dependent on contrast agent concentration. In order to accurately quantify fMBV, water exchange must be simultaneously determined using a multi-compartmental model. The interplay between fMBV and water exchange based on T1 measurements is described in Appendix 2 (6, 7, 18, 19).

Using a two-compartment model of the myocardium, which divides a unit of tissue into an intravascular compartment (composed of plasma and red blood cells) and an extravascular compartment (composed of the interstitium, myocytes, and other cells) (6), the fMBV can be estimated. Figure 1 illustrates a 2-compartmental model of myocardial tissue and spin interactions along with respective representative rate constants. In the 2-compartmental model, the intravascular and extravascular compartments represent separate relaxation environments, in which the longitudinal relaxation time constant R1 of unbound water protons differs as a result of exposure to the intravascular contrast agent. In this formulation,

an excited water proton spin will spend some fraction τ_i of time in the intravascular compartment, and some fraction τ_e in the extravascular compartment. These residence times (τ_i and τ_e) are inversely related to the intercompartmental exchange rates k_i and k_e, the rates at which water enters the respective compartments. A single excited spin is exposed to a relaxation environment with $R1_i$ during the time it spends in the intravascular compartment and $R1_e$ during its time in the extravascular compartment. As a result, the overall relaxation rate of the myocardial tissue is influenced by the water relaxation rate of each compartment. On the scale of a population of spins in a two-compartment system, the longitudinal relaxation of the bulk magnetization following an excitation pulse can be described by a biexponential function, as formulated by Bjornerud et al (19). While water also diffuses into and out of cells in both compartments, transcytolemmal water exchange has been shown to be sufficiently fast relative to vascular exchange to justify a two-compartment, single-exchange model (7, 20–22).

Applying Bjornerud et al. and Schwarzbauer's blood volume model (18, 19) (see Appendix 2) to our current approximations of fMBV using ferumoxytol as an intravascular contrast agent, the observed longitudinal relaxation rate of myocardial tissue ($R1_{myo}$) is modeled as a function of five parameters: 1) the intravascular longitudinal relaxation rate ($R1_i$), 2) the myocardial extravascular longitudinal relaxation rate ($R1_e$), 3) the fMBV, 4) the intravascular water exchange rate k_i, and 5) the tissue-blood partition coefficient ($\lambda = \rho/\rho_i$, the ratio of the proton spin densities of tissue and blood). fMBV is related to k_i and the extravascular water exchange rate k_e by the expression

$$fMBV = \lambda \frac{k_e}{k_e + k_i}. \quad (1)$$

$R1_{myo}$ and $R1_i$ can be obtained from myocardial T1 maps acquired at steady state over a range of cumulative ferumoxytol doses. These repeated measurements of $R1_{myo}$ and $R1_i$ can be plotted and describe the ferumoxytol dose response of the myocardium and LV blood pool. After constructing these dose-response curves (whole myocardium or segmental), a constrained nonlinear multivariable optimization solver can be used to find the point (fMBV, $R1_e$, k_i, λ) that minimizes the sum of squared error between the calculated $R1_{myo}$' and the measured $R1_{myo}$ (23–25).

Estimation of Extravascular T1 ($T1_e$) from Imaging Data

Two-compartment models of fMBV typically fit four parameters (fMBV, $R1_e$, k_i, λ) to a measured dose response curve ($R1_{myo}$, $R1_i$). Consistent with the principle of parsimony whereby the least number of parameters that adequately describe the phenomena is recommended (26), we developed a method to estimate $R1_e$ directly from the ($R1_{myo}$, $R1_i$) curve in order to use a three- rather than four-parameter fit. We assumed that the intravascular compartment of the myocardial tissue (the volume of blood in the capillary bed) and the LV blood pool had equal R1 relaxivity at contrast steady state; the time to steady-state duration was determined in a pilot study and is outlined in the section on image acquisition. As the cumulative ferumoxytol dose was increased such that the $R1_i$ matched $R1_e$, the contrast between the myocardium and LV blood pool was nulled ($R1_e = R1_{myo} =$

$R1_i$). As the cumulative ferumoxytol dose was further increased, the blood pool-myocardium contrast was inverted. We estimated $R1_e$ by performing a simple linear interpolation to find the intersection of the blood and myocardial segmental ferumoxytol dose-response curves. This treatment assumed that $R1_e$ was uniform throughout the myocardium and independent of ferumoxytol dose. While this method ignored the effect of water exchange on $T1_e$ as the ferumoxytol dose was increased, the crossover of blood and myocardial T1 occurs in the low dose range where the fast-exchange assumption is more applicable. This method allowed us to fit three parameters rather than four, thus simplifying the two-compartment model.

Experimental Animal Care And Use

After obtaining approval from our Institutional Animal Care and Use Committee, we conducted all animal studies in adherence to the recommendations of the Guide for the Care and use of Laboratory Animals, the Animal Welfare Act, the National Institutes of Health, and the American Heart Association (AHA) on Research Animal Use (adopted November 11, 1984). Ten 22-46 kg, adult male Yorkshire swine (S&S Farms, Ramona, CA) were housed in a dedicated vivarium staffed by certified veterinarians for two weeks prior to experiments.

We used intramuscular ketamine (10mg/kg), midazolam (1mg/kg), and inhaled 1-2% isoflurane to achieve sedation and anesthesia of swine subjects. To minimize respiratory motion artifacts, we used intravenous rocuronium (2.5mg/kg/hr) to immobilize the diaphragm during anesthesia. Swine were ventilated with an oxygen-isoflurane mixture (1-2%) and a surgical plane of anesthesia was maintained. Hemodynamic and electrocardiographic vital signs were monitored throughout all procedures by two certified Veterinary Technicians and a board-certified cardiologist (KLN).

We artificially induced a focal coronary stenosis in the mid left anterior descending (LAD) artery of one swine subject using a percutaneously deployed 3D printed, heparin-coated, coronary implant in a closed-chest model (27, 28). We acquired orthogonal X-ray contrast angiograms to locate and assess the severity of the stenosis. To prevent thrombus formation, we administered a bolus of heparin (10,000 units) prior to the start of the procedure and subsequently maintained an activated clotting time above 300 seconds with intravenous heparin throughout the imaging study. After confirmation of coronary stenosis on coronary angiography, we began the MRI study within 60 minutes.

Image Acquisition

To determine the time to steady-state distribution of ferumoxytol in vivo, in a preliminary study in two separate healthy, normal swine subjects, we sequentially measured mid-ventricular myocardial and LV blood pool T1 once per minute following ferumoxytol infusion (4mg/kg). T1 maps using the 5(3)3(3)3 Modified Look-Locker Inversion (MOLLI) recovery sequence (29) with a balanced steady-state free precession (bSSFP) readout were acquired: [FOV = 240 x 300 mm, matrix size = 384 x 308, TR = 2.6 ms, TE = 1.08 ms, slice thickness = 8 mm, pixel bandwidth = 1085 Hz, flip angle = 35°, TI = 100 – 180 ms].

For the core experiments in this paper, after anesthesia alone (N=9) or anesthesia and coronary implant deployment (N=1), we transferred the swine subjects to a whole body

clinical 3.0 T magnet (Prisma®, Siemens Medical Solutions USA, Malvern, PA) equipped with phased-array coils. Following localizers, we performed a ferumoxytol multi-dose T1 mapping study (Figure 2). We acquired non-contrast short-axis T1 maps using the 5(3)3(3)3 Modified Look-Locker Inversion (MOLLI) recovery sequence (29) with a balanced steady-state free precession (bSSFP) readout in the mid left ventricle in all healthy, normal swine (N=9), and in the left ventricular apex in the single instrumented swine model (N=1) [FOV = 240 x 300 mm, matrix size = 384 x 308, TR = 2.6 ms, TE = 1.08 ms, slice thickness = 8 mm, pixel bandwidth = 1085 Hz, flip angle = 35°, TI = 100 – 180 ms]. After native (non-contrast) imaging, we administered a cumulative ferumoxytol dose of 4.0 mg/kg over multiple infusions (cumulative dose 0.25, 0.5, 1.0, 2.0, 3.0 and 4.0 mg/kg, 20-fold dilution) at a rate of 0.33 mg/kg/min. Informed by results from our preliminary work on time to steady-state distribution of ferumoxytol in vivo, we observed a five-minute delay following each incremental ferumoxytol dose prior to T1 MRI in order to ensure contrast steady state. The MOLLI T1 mapping pulse sequence was repeated in the same short-axis slice after a five-minute delay following each dose of ferumoxytol (FOV = 240 x 300 mm, matrix size = 384 x 308, TR = 2.6 ms, TE = 1.08 ms, slice thickness = 8 mm, pixel bandwidth = 1085 Hz, flip angle = 35°, TI = 100 – 180 ms). Following a preliminary analysis, we added an additional dose at 0.125 mg/kg in the latter four swine subjects in order to more densely sample the low-dose range. The typical total duration of the ferumoxytol multi-dose imaging study was approximately 55 minutes. For all FE T1 acquisitions following the initial native T1 acquisition, we used a MOLLI sequence with inversion times optimized for shorter post-contrast T1 relaxation time. After imaging, healthy normal swine subjects were transferred to an invasive protocol.

Image Processing

We used the Instantaneous Signal Loss simulation (InSiL) algorithm with an inversion factor of 96% for T1 fitting of MOLLI images in order to minimize T1 error at high heart rates (>80 bpm) (30). Using commercially available software (Osirix, Pixmeo, Bernex, Switzerland), we contoured and segmented each mid-ventricular MOLLI InSiL-fitted T1 map into six segments based on the AHA 17-segment model, and excluded segments with severe artifacts (CMC, 3 years cardiovascular MRI experience; contours confirmed by KLN, >9 years cardiovascular MRI experience) (31). We contoured a central region of the mid-LV blood pool with careful attention to exclusion of trabeculation and papillary muscles. In raw images with visible motion artifacts, we manually fitted myocardial segmental T1 using InSiL. We exported segmental myocardial ferumoxytol ($R1_{myo,}$ $R1_i$) curves to MATLAB (MathWorks, Natick, MA) for fMBV modelling. We estimated $R1_e$ as described above and fitted fMBV, k_i and λ for the whole myocardium and for each myocardial segment for all subjects.

We used the two-compartment water exchange model to generate pixel-wise fMBV maps of one healthy swine and one swine with artificially induced myocardial hypoperfusion. In order to capture the full extent of myocardial hypoperfusion downstream from the intracoronary stenosis implant, fMBV was measured in the left ventricular apex in the instrumented swine model. Prior to fMBV fitting, we co-registered the set of eight InSiL T1 maps generated at each cumulative ferumoxytol dose (0-4.0 mg/kg) using a groupwise

image registration method designed for parametric mapping applications in Elastix (5.0.0) (32, 33). Using the $R1_i$ and $R1_e$ derived from segmental data, we computed fMBV and intravascular water exchange for each pixel using a three-parameter fit. We segmented the pixel-wise fMBV maps into 6 segments (normal swine subject, mid slice) and 4 segments (instrumented swine subject, apical slice) respectively, based on the AHA 17-segment model.

Comparison of fMBV to Other Proxies of Blood Volume Estimation and Identification of an Optimized Ferumoxytol Dosing and Sampling Scheme

Due in part to the long exam time required for performance of a multi-dose T1 acquisition, several simplified surrogates of blood volume have been proposed. We evaluated fast-exchange fMBV (equation 1–2) in nine normal swine subjects in order to assess its agreement with our model-fitted fMBV. R1 subtraction maps have also been proposed as a substitute for model-fitted blood volume because change in tissue R1 is related to local blood volume fraction (34). We evaluated the percent increase in myocardial R1, $(\frac{R1_{post\ ferumoxytol} - R1_{pre\ ferumoxytol}}{R1_{pre\ ferumoxytol}})$, following a cumulative ferumoxytol infusion of 4.0 mg/kg.

In order to optimize the number of ferumoxytol infusions necessary for accurate quantification of fMBV using the two-compartment model, we evaluated segmental fMBV in four swine subjects using various dose under-sampling schemes with three parameter fitting. Each under-sampled scheme used four doses out of the complete set of eight that were acquired. In order to capture the full range of the ($R1_{myo,}$ $R1_i$) curve, each four-dose scheme included the minimum and maximum ferumoxytol dose (0.0 and 4.0 mg/kg), with two additional doses in the intermediate range (0.125 to 3.0 mg/kg).

Statistical Analysis

We used the Kolmogorov-Smirnov test to assess data normality. Normally distributed data are represented as mean ± standard deviation (SD). Following contouring of myocardial T1 maps in accordance with the AHA 17-segment model and fitting of fMBV, we used one-way analysis of variance (ANOVA) to assess variation in fMBV between subjects and between myocardial segments. We generated Bland-Altman plots to assess agreement of image-derived and model-fitted $T1_e$. We assessed the agreement between 1) fast-exchange fMBV (equation 1–2) and our model-fitted fMBV estimates; and 2) fMBV fitted to under-sampled (4 doses) curves relative to our fully sampled (8 doses), model-fitted fMBV. We used Pearson R-correlation to determine the relationship between fMBV and percent-increase in myocardial R1. We performed statistical analyses in MATLAB and MedCalc (v19.0.5, MedCalc Software, Ostend, Belgium). A p value < 0.05 was considered statistically significant.

RESULTS

Ferumoxytol Dose-Response of LV Blood Pool and Myocardial T1

Myocardial and LV blood pool T1 reached steady state within three to four minutes following ferumoxytol infusion in a preliminary study in two swine subjects. Ferumoxytol dose-response of myocardial and blood pool T1 is summarized in Figure 3. Prior to ferumoxytol infusion, the myocardium and LV blood pool at 3.0T showed a mean native T1 of 1389 ± 23 ms and 1846 ± 73 ms, respectively. Mean myocardial and LV blood pool T1 decreased monotonically with increasing ferumoxytol dose. The multi-dose T1 imaging study captured the inversion of contrast between the myocardium and LV blood pool between 0.125 mg/kg and 0.25 mg/kg of ferumoxytol. Following the cumulative infusion of 4.0 mg/kg, we found a steady state mean myocardial and blood pool T1 of 832 ± 26 ms and 115 ± 10 ms, respectively. No ferumoxytol-related adverse events occurred, and vital signs were stable throughout the course of the exams.

Image-Derived and Model-Fitted Extravascular T1

We found a mean image-derived extravascular T1 of 1328 ± 35 ms and a mean model-fitted extravascular T1 of 1331 ± 27 ms. The mean percent-difference between the two extravascular T1 estimates across all subjects was 0.28 ± 0.95%. Bland-Altman analysis found no significant bias (p=0.409, n=9) and limits of agreement (LOA) of −20.9 ms [95% CI −38.0, −3.79 ms] to 28.2 [11.07, 45.30 ms].

Segmental fMBV and Water Exchange

We quantified segmental fMBV and water exchange in the mid-ventricular myocardium of all swine subjects using a two-compartment model with three-parameter curve fitting and image-derived extravascular T1. The constrained nonlinear multivariable optimization solver was able to converge to a solution for all segments in all subjects. Model-generated ($R1_{myo,}$ $R1_i$) curves fit the imaging data well, with a median R^2 of 0.997 (IQR 0.992 – 0.998; range 0.919 – 1.000). We found a mean mid-ventricular fMBV of 7.2 ± 1.4% and a mean intravascular water exchange rate of 11.3 ± 5.1 s^{-1}. These results are presented alongside the results of similar published methods in Table 1.

One-way ANOVA across nine healthy swine subjects showed significant variance in global fMBV between subjects (7.95 ± 2.00%, 7.25 ± 2.92%, 8.07 ± 1.38%, 9.59 ± 2.21%, 7.80 ± 1.44%, 5.93 ± 1.43%, 6.84 ± 0.65%, 5.78 ± 2.05%, 8.31 ± 1.94%; $p < 0.05$), indicating that individual normal swine subjects can present with slightly different baseline fMBV. We performed one-way ANOVA across the six mid-ventricular myocardial segments in this population of normal swine subjects to evaluate whether an underlying pattern of variation in fMBV existed among coronary territories. One-way ANOVA showed no significant variance in fMBV across the six mid-ventricular coronary territories (8.60 ± 2.95% [anterior], 7.61 ± 2.56% [anteroseptal], 6.91 ± 1.80% [inferoseptal], 7.74 ± 1.85% [inferior], 6.84 ± 1.49% [inferolateral], 7.30 ± 1.43% [anterolateral]; p=0.387). Figure 4 summarizes fMBV across the mid myocardial segments in the nine healthy swine subjects. There was no significant correlation between global fMBV and total body mass across all subjects (p=0.117).

Comparison of Model-Fitted fMBV to Other Proxies of Blood Volume Estimation

Fast-exchange fMBV computed at 2.0 mg/kg ferumoxytol showed the best nominal agreement with model-fitted fMBV (Appendix 3). Linear regression analysis showed a moderate correlation between fast-exchange fMBV at 2.0 mg/kg and model-fitted fMBV ($r = 0.71$, $p < 0.05$). Bland-Altman analysis of the fast-exchange vs model fitted fMBV found LOA of −2.60% [−3.29, −1.92%] to 2.76% [2.08, 3.45%] without significant bias (mean difference=0.08, p=0.688, Figure 5). Linear regression also showed a significant, but poor correlation between percent-change in R1 following ferumoxytol infusion of 4.0 mg/kg and model-fitted fMBV ($r=0.50$, $p < 0.05$).

Optimized Sampling Scheme and Ferumoxytol Dosing for fMBV Quantification

The optimal dosing scheme that maximized the agreement of fMBV derived from the under-sampled and the complete dataset was 0.0, 0.125, 2.0, and 4.0 mg/kg ferumoxytol. Linear regression analysis showed significant and strong positive correlation between fMBV estimates from the under-sampled and the complete dataset ($r=0.95$, $p < 0.05$). Bland-Altman analysis of under-sampled relative to the complete dataset for fMBV showed LOA of −1.04% [−1.45, −0.62%] to 1.18% [0.77, 1.59%] without significant bias (mean difference=0.07, p=0.541, Figure 6). When extravascular T1 was fitted as a model parameter in both the complete and under-sampled datasets, the same dose under-sampling scheme showed a strong correlation ($r=0.97$, $p < 0.05$), no significant bias (mean difference=0.19, p=0.08), and fMBV LOA of −0.80% [−1.16, −0.43%] to 1.17% [0.80, 1.53%].

Pixel-Wise Myocardial Blood Volume

We used our two-compartment water exchange model to generate pixel-wise fMBV maps for a swine subject with myocardial hypoperfusion in the mid to distal LAD coronary territory, as well as a single healthy, normal swine subject (Figure 7). Pixel-wise fMBV for each myocardial segment is reported in Table 2. In the swine with artificially-induced stenosis of the LAD, we found a mean pixelwise fMBV of 11.90 ± 4.00%, 16.10 ± 5.71%, 9.59 ± 3.35%, and 9.38 ± 2.35% in the anterior, septal, inferior and lateral segments respectively. Quantitative pixel-wise fMBV showed regional differences in hypoperfused relative to perfused segments. When fMBV is plotted on colorized maps as in Figure 7, this difference is readily visible in the segments that are hypoperfused by the stenotic LAD.

DISCUSSION

Our study demonstrated the feasibility of fMBV quantification from FE-MRI using a two-compartment water exchange model with three-parameter curve fitting in nine healthy, normal swine subjects and a single swine with artificially-induced coronary stenosis. We showed that extravascular T1 can be derived directly from imaging data to simplify the model. Although simple linear interpolation of extravascular T1 from imaging data ignores the effect of water exchange on extravascular T1, an assumption that we avoided elsewhere in our fMBV model, we have shown empirically that extravascular T1 values extracted directly from imaging data match closely with values derived from four-parameter curve fitting. To further facilitate clinical translation of the proposed work, we also identified a

sparser dose sampling scheme that maintained the accuracy of fMBV estimates. These findings have important clinical implications for the characterization of tissue perfusion.

Several other approaches have been proposed to estimate fMBV, including simple fast-exchange fMBV (equation 1–2) and percent change in R1 (pre and post contrast). Although our calculations showed good correlation between simple fast-exchange fMBV and model-fitted fMBV, Bland-Altman analysis showed wide limits of agreement which may obscure subtle changes in regional myocardial hypoperfusion. On the other hand, percent change in R1 following 4 mg/kg ferumoxytol showed a weaker correlation with model-fitted fMBV and is likely to be least useful clinically. In the clinical setting, where patients frequently present with multi-vessel disease, we expect to observe a wide degree of heterogeneity in ischemia severity across myocardial segments within individual patients. We also expect a greater incidence of respiratory motion artifacts. As a result, a relatively sensitive imaging biomarker is desired. While the fast-exchange fMBV approach and the percent change in R1 methods are simple, they are less promising as reliable surrogates for fMBV. Further comparisons should be made in the clinical setting, where disease is more nuanced, to confirm our hypothesis.

Little has been published about the minimum number of contrast doses needed to accurately model fMBV, and published studies employ a range of sampling schemes (18, 19, 35). Among the under-sampling schemes tested, the (0.0, 0.125, 2.0, and 4.0 mg/kg ferumoxytol) scheme showed closest agreement with the fully-sampled scheme. When compared to the difference in fMBV between perfused and hypoperfused myocardial segments in a single instrumented swine model, the small limits of agreement with this scheme suggested that differentiation of regional myocardial hypoperfusion using model-fitted fMBV may be feasible with four T1 acquisitions rather than eight. This dose sampling scheme would reduce the total study time to approximately 35 minutes – comparable to the duration of a typical stress perfusion MRI study. These results are promising, as long exam times and complex acquisition protocols can deter clinical adoption of new imaging approaches.

Multi-compartmental modelling with intravascular contrast agents has been used to investigate fMBV in healthy volunteers, patients, and large animal models (17, 19, 35), but data using clinically available intravascular contrast agents such as ferumoxytol are limited (17). The published literature reflects a range of contrast agents, dosages, T1 imaging pulse sequences and fitting algorithms (17, 19, 35). A comparison between our fMBV estimation and a selection of similar published methods (17, 19, 35) demonstrates a range of complexity for both compartmental models and acquisition protocols. Our two-compartment model is moderately complex relative to other published methods (17, 19, 35). Pixel-wise mapping of fMBV using our method requires the extraction of blood and whole-myocardial R1 prior to fMBV fitting. While our imaging protocol required the acquisition of eight individual MOLLI images, our dose optimization study found that a four-dose protocol may perform comparably well.

Published fMBV values range from 5% to 12% and water exchange rates range from 8.5 to 14.2 s^{-1} in human, swine and canine studies using the iron-based intravascular contrast agents ferumoxytol and NC100150 (17, 19). Our segmental fMBV and water exchange

results in nine healthy swine models fall within the published ranges. McCommis et al. found an absolute MBV of 6.1 ± 0.5 mL/100g in healthy canine subjects using first pass perfusion MRI with a dendritic gadolinium-based contrast agent (36) that has intravascular properties, which correlated well with their reference MBV values derived from red blood cell radiolabeling. Differences between our fMBV values and those from McCommis et al may relate to differences in contrast agents, subject population, imaging pulse sequence, and model fitting. We employed a true intravascular indicator, ferumoxytol, which has an intravascular residence time of 10-15 hours in healthy vasculature. Most clinically available gadolinium-chelates are extracellular agents that leak into the extravascular space. Even when extravasation is taken into account during modeling (17), the use of extracellular agents may be less desirable for steady-state fractional blood volume modelling.

Our fMBV values using a two-compartment water exchange model based on FE-MRI in a swine with a focal LAD stenosis are hypothesis-generating. We found that increased fMBV in the myocardial segment perfused by the stenosed LAD (septum) relative to remote segments. Elevated fMBV has been proposed as a compensatory response in the setting of regional myocardial hypoperfusion downstream from a significant coronary stenosis (5) and our interesting observation in a swine model with artificially-induced regional myocardial hypoperfusion complements work by McCommis et al. who measured MBV in dogs with first pass perfusion imaging (36). Further work is underway to closely evaluate this finding.

Limitations

First, our model-fitted fMBV has been derived using data obtained with a specific intravascular contrast agent (ferumoxytol) in combination with a specific MOLLI derived T1 mapping sequence. Second, our model of fMBV was based on only nine healthy normal swine subjects and one swine with moderate to severe LAD coronary stenosis. While we obtained mean segmental fMBV within the range of published values for similar studies conducted in humans and large animals, the broad range of published contrast doses, imaging pulse sequences and fitting algorithms complicates one-to-one comparison of methodologies. Likewise, we chose to implement a two- , rather than three-compartment model, ignoring the effects of transcytolemmal water exchange. Third, while anesthesia enables high quality pixelwise fMBV mapping in this preclinical study, respiratory motion will pose a greater challenge in the clinical setting. Likewise, Baudelet et al. found that intraperitoneal ketamine (80 mg/kg) significantly reduced perfusion of skeletal muscle in a mouse liver tumor model (37). While the ketamine dose used in our swine protocol (10 mg/kg, intramuscular) was much less, it is possible that intramuscular ketamine could result in a slight reduction in myocardial perfusion in this swine model, affecting measured fMBV. Fourth, we did not compare our model-fitted fMBV to other reference techniques. Nevertheless, our model-fitted fMBV values aligned with published values for fMBV in swine models using MRI. We evaluated our pixel-wise blood volume mapping technique in a single instrumented swine model, rather than in a clinical study, in order to eliminate artifacts due to respiratory motion and precisely control the degree and location of single-vessel coronary stenosis. This allowed us to directly compare fMBV in ischemic and remote myocardial regions, while ensuring the highest possible quality of T1 and fMBV maps in the proof-of-concept stage. Our preliminary observation of elevated fMBV in the myocardial

territory perfused by the LAD is promising and provides very early evidence that tissue blood volume could potentially be used to discriminate between hypoperfused relative to perfused tissues (5, 17). However, these findings clearly require further study and validation. Last, while the safety profile for off-label, diagnostic use of ferumoxytol is favorable to date (9, 38, 39), there remains a rare risk for severe hypersensitivity reactions associated with the use of intravenous iron agents.

Conclusion

Two-compartment modelling for estimation of fMBV is feasible using steady-state MOLLI T1 mapping over multiple doses of the clinically available iron-based intravascular agent ferumoxytol. fMBV derived from FE-MRI may have the potential to provide a unique means of assessing myocardial perfusion, particularly in settings where renal function may preclude the use of gadolinium-based agents. If confirmed in patients, model-fitted fMBV may serve as a potential direct marker of myocardial tissue perfusion.

Supplementary Material

Refer to Web version on PubMed Central for supplementary material.

Acknowledgements

We thank staff members at the UCLA Lux Lab, the UCLA Translational Research Imaging Center (TRIC) and the Division of Laboratory Animal Medicine at UCLA for their assistance.

Funding:

This work is supported by American Heart Association Transformational Award 18TPA34170049 and the National Heart, Lung, and Blood Institute R01HL148182.

References

1. Peters AM: Fundamentals of tracer kinetics for radiologists. Br J Radiol 1998(NOV.):1116–1129. [PubMed: 10434905]
2. Koh TS, Bisdas S, Koh DM, Thng CH: Fundamentals of tracer kinetics for dynamic contrast-enhanced MRI. J Magn Reson Imaging 2011:1262–1276.
3. Ewing JR, Bagher-Ebadian H: Model selection in measures of vascular parameters using dynamic contrast-enhanced MRI: Experimental and clinical applications. NMR Biomed 2013; 26:1028–1041. [PubMed: 23881857]
4. McCommis KS, Goldstein TA, Abendschein DR, et al.: Roles of myocardial blood volume and flow in coronary artery disease: an experimental MRI study at rest and during hyperemia. Eur Radiol 2010; 20:2005–2012. [PubMed: 20182731]
5. Lindner JR, Skyba DM, Goodman NC, Jayaweera AR, Kaul S: Changes in myocardial blood volume with graded coronary stenosis. Am J Physiol 1997; 272(1 Pt 2):H567–75. [PubMed: 9038980]
6. Hazlewood CF, Chang DC, Nichols BL, Woessner DE: Nuclear Magnetic Resonance Transverse Relaxation Times of Water Protons in Skeletal Muscle. Biophys J 1974; 14:583–606. [PubMed: 4853385]
7. Donahue KM, Weisskoff RM, Chesler DA, et al.: Improving MR quantification of regional blood volume with intravascular T1 contrast agents: Accuracy, precision, and water exchange. Magn Reson Med 1996; 36:858–867. [PubMed: 8946351]

8. Bullivant JP, Zhao S, Willenberg BJ, Kozissnik B, Batich CD, Dobson J: Materials characterization of feraheme/ferumoxytol and preliminary evaluation of its potential for magnetic fluid hyperthermia. Int J Mol Sci 2013; 14:17501–17510. [PubMed: 24065092]

9. Nguyen K-L, Yoshida T, Kathuria-Prakash N, et al.: Multicenter Safety and Practice for Off-Label Diagnostic Use of Ferumoxytol in MRI. Radiology 2019:190477.

10. Han F, Rapacchi S, Khan S, et al.: Four-dimensional, multiphase, steady-state imaging with contrast enhancement (MUSIC) in the heart: A feasibility study in children. Magn Reson Med 2015; 74:1042–1049. [PubMed: 25302932]

11. Nguyen K-L, Park EA, Yoshida T, Hu P, Finn JP: Ferumoxytol enhanced black-blood cardiovascular magnetic resonance imaging. J Cardiovasc Magn Reson 2017; 19. [PubMed: 28183320]

12. Stirrat CG, Alam SR, MacGillivray TJ, et al.: Ferumoxytol-enhanced magnetic resonance imaging assessing inflammation after myocardial infarction. Heart 2017; 103:1528–1535. [PubMed: 28642288]

13. Ramasawmy R, Rogers T, Alcantar MA, et al.: Blood volume measurement using cardiovascular magnetic resonance and ferumoxytol: preclinical validation. J Cardiovasc Magn Reson 2018; 20:62. [PubMed: 30201013]

14. Knobloch G, Colgan T, Schiebler ML, et al.: Comparison of gadolinium-enhanced and ferumoxytol-enhanced conventional and UTE-MRA for the depiction of the pulmonary vasculature. Magn Reson Med 2019; 82:1660–1670. [PubMed: 31228293]

15. Li W, Tutton S, Vu AT, et al.: First-pass contrast-enhanced magnetic resonance angiography in humans using ferumoxytol, a novel ultrasmall superparamagnetic iron oxide (USPIO)-based blood pool agent. J Magn Reson Imaging 2005; 21:46–52. [PubMed: 15611942]

16. Knobloch G, Colgan T, Wiens CN, et al.: Relaxivity of ferumoxytol at 1.5T and 3.0T HHS Public Access. Invest Radiol 2018; 53:257–263. [PubMed: 29215401]

17. Bane O, Lee DC, Benefield BC, et al.: Leakage and water exchange characterization of gadofosveset in the myocardium. Magn Reson Imaging 2014; 32:224–235. [PubMed: 24418327]

18. Schwarzbauer C, Morrissey SP, Deichmann R, et al.: Quantitative magnetic resonance imaging of capillary water permeability and regional blood volume with an intravascular MR contrast agent. Magn Reson Med 1997; 37:769–777. [PubMed: 9126952]

19. Bjørnerud A, Bjerner T, Johansson LO, Ahlström HK: Assessment of myocardial blood volume and water exchange: Theoretical considerations and in vivo results. Magn Reson Med 2003; 49:828–837. [PubMed: 12704765]

20. Sobol WT, Jackels SC, Cothran RL, Hinson WH: NMR spin-lattice relaxation in tissues with high concentration of paramagnetic contrast media: Evaluation of water exchange rates in intact rat muscle. Med Phys 1991; 18:243–250. [PubMed: 2046611]

21. Wedeking P, Sotak CH, Telser J, Kumar K, Chang CA, Tweedle MF: Quantitative dependence of MR signal intensity on tissue concentration of Gd(HP-DO3A) in the nephrectomized rat. Magn Reson Imaging 1992; 10:97–108. [PubMed: 1545688]

22. Donahue KM, Burstein D, Manning WJ, Gray ML: Studies of Gd-DTPA relaxivity and proton exchange rates in tissue. Magn Reson Med 1994; 32:66–76. [PubMed: 8084239]

23. Byrd RH, Gilbert JC, Nocedal J: A trust region method based on interior point techniques for nonlinear programming. Math Program Ser B 2000; 89:149–185.

24. Waltz RA, Morales JL, Nocedal J, Orban D: An interior algorithm for nonlinear optimization that combines line search and trust region steps. Math Program 2006; 107:391–408.

25. Ugray Z, Lasdon L, Plummer J, Glover F, Kelly J, Marti R: Scatter search and local NLP solvers: A multistart framework for global optimization. INFORMS J Comput 2007; 19:328–340.

26. Ratkowsky DA: Principles of nonlinear regression modeling. J Ind Microbiol 1993; 12:195–199.

27. Hollowed JJ, Colbert CM, Currier JW, Nguyen K-L: Novel Percutaneous Approach for Deployment of 3D Printed Coronary Stenosis Implants in Swine Models of Ischemic Heart Disease. J Vis Exp 2020:e60729.

28. Colbert CM, Shao J, Hollowed JJ, et al.: 3D-Printed Coronary Implants Are Effective for Percutaneous Creation of Swine Models with Focal Coronary Stenosis. J Cardiovasc Transl Res 2020:1–11. [PubMed: 31942675]

29. Messroghli DR, Greiser A, Fröhlich M, Dietz R, Schulz-Menger J: Optimization and validation of a fully-integrated pulse sequence for modified look-locker inversion-recovery (MOLLI) T1 mapping of the heart. J Magn Reson Imaging 2007; 26:1081–1086. [PubMed: 17896383]

30. Shao J, Nguyen K-L, Natsuaki Y, Spottiswoode B, Hu P: Instantaneous signal loss simulation (InSiL): An improved algorithm for myocardial T1 mapping using the MOLLI sequence. J Magn Reson Imaging 2015; 41:721–729. [PubMed: 24677371]

31. Cerqueira MD, Weissman NJ, Dilsizian V, et al.: Standardized myocardial segmentation and nomenclature for tomographic imaging of the heart: A Statement for Healthcare Professionals from the Cardiac Imaging Committee of the Council on Clinical Cardiology of the American Heart Association. Circulation 2002:539–542.

32. Klein S, Staring M, Murphy K, Viergever MA, Pluim JPW: Elastix: A toolbox for intensity-based medical image registration. IEEE Trans Med Imaging 2010; 29:196–205. [PubMed: 19923044]

33. Huizinga W, Poot DHJ, Guyader JM, et al.: PCA-based groupwise image registration for quantitative MRI. Med Image Anal 2016; 29:65–78. [PubMed: 26802910]

34. Niendorf T, Seeliger E, Cantow K, Flemming B, Waiczies S, Pohlmann A: Probing renal blood volume with magnetic resonance imaging. Acta Physiol 2019(12 2019):1–14.

35. Wacker CM, Wiesmann F, Bock M, et al.: Determination of regional blood volume and intra-extracapillary water exchange in human myocardium using Feruglose: First clinical results in patients with coronary artery disease. Magn Reson Med 2002; 47:1013–1016. [PubMed: 11979582]

36. McCommis KS, Goldstein TA, Zhang H, Misselwitz B, Gropler RJ, Zheng J: Quantification of myocardial blood volume during dipyridamole and doubtamine stress: a perfusion CMR study. J Cardiovasc Magn Reson 2007; 9:785–792. [PubMed: 17891616]

37. Baudelet C, Gallez B: Effect of anesthesia on the signal intensity in tumors using BOLD-MRI: Comparison with flow measurements by Laser Doppler flowmetry and oxygen measurements by luminescence-based probes. Magn Reson Imaging 2004; 22:905–912. [PubMed: 15288130]

38. Toth GB, Varallyay CG, Horvath A, et al.: Current and potential imaging applications of ferumoxytol for magnetic resonance imaging. Kidney Int 2017:47–66. [PubMed: 28434822]

39. Vasanawala SS, Nguyen KL, Hope MD, et al.: Safety and technique of ferumoxytol administration for MRI. Magn Reson Med 2016; 75:2107–2111. [PubMed: 26890830]

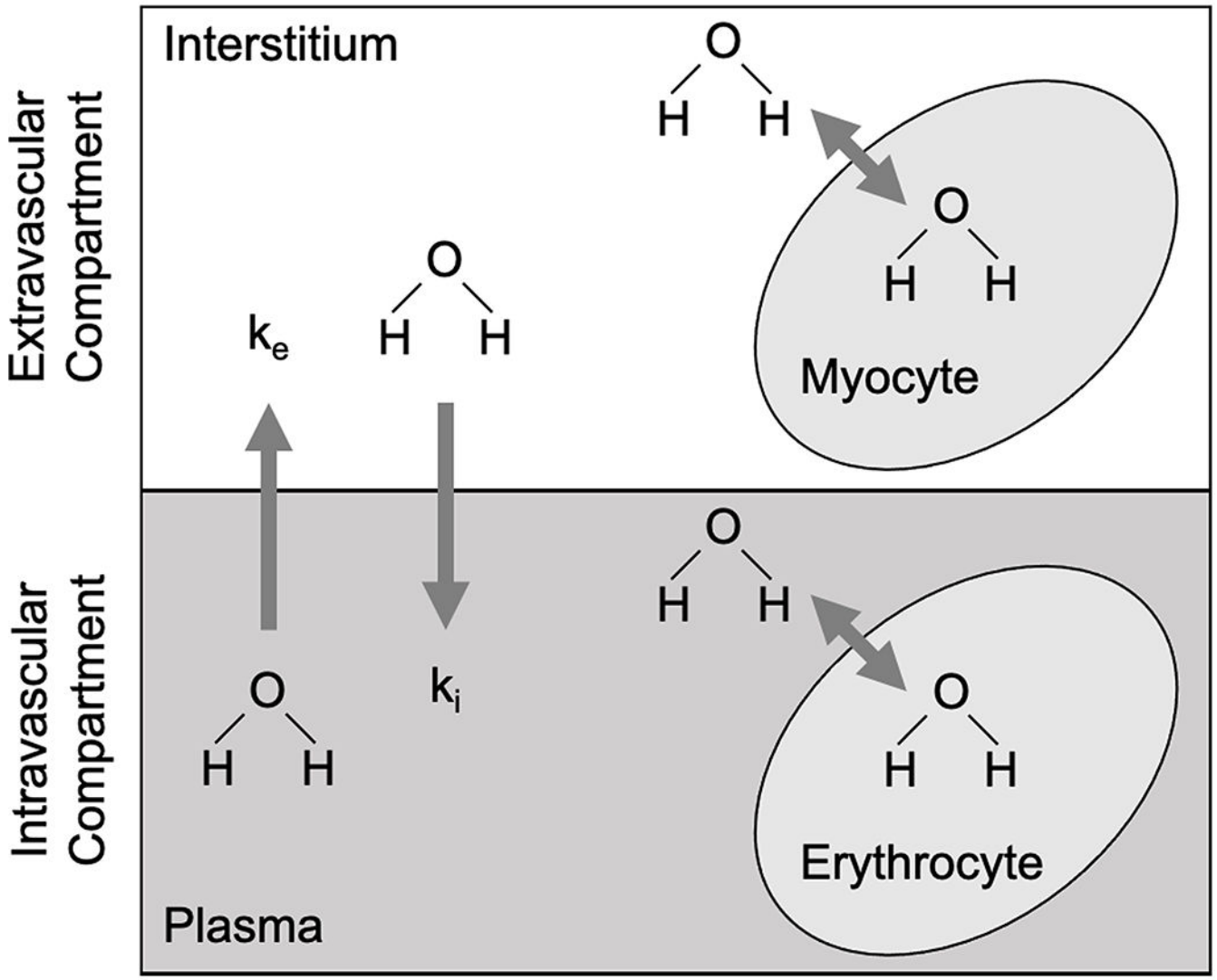

FIGURE 1.

Illustration of spin relaxation environments included in multi-compartmental models of myocardial tissue. Two-compartment water exchange models account for water exchange between intravascular and extravascular environments, without accounting for transcytolemmal water exchange. k_e, extravascular water exchange rate; k_i, intravascular water exchange rate.

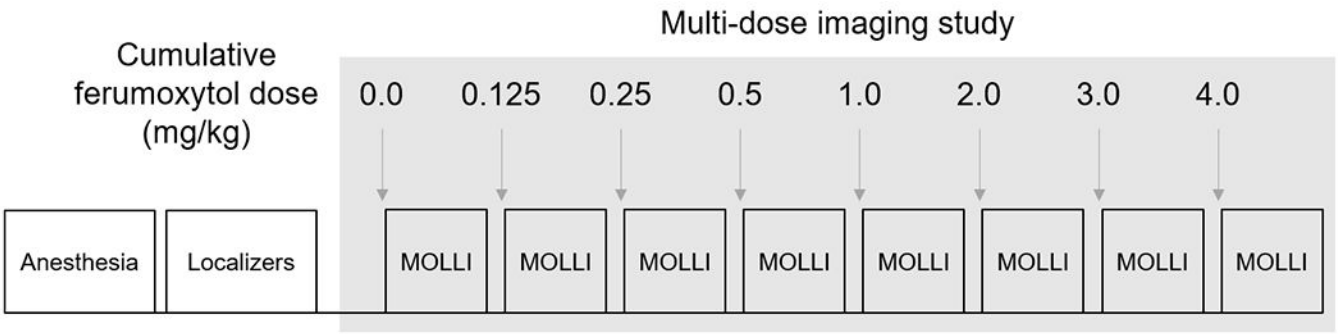

FIGURE 2.

Ferumoxytol multi-dose T1 mapping study protocol. Following anesthesia and localizers, we acquired mid-ventricular short axis T1 maps at eight cumulative ferumoxytol doses (0.0 – 4.0 mg/kg). Following each ferumoxytol infusion, we observed a five-minute delay to achieve contrast steady state. MOLLI, Modified Look-Locker Inversion.

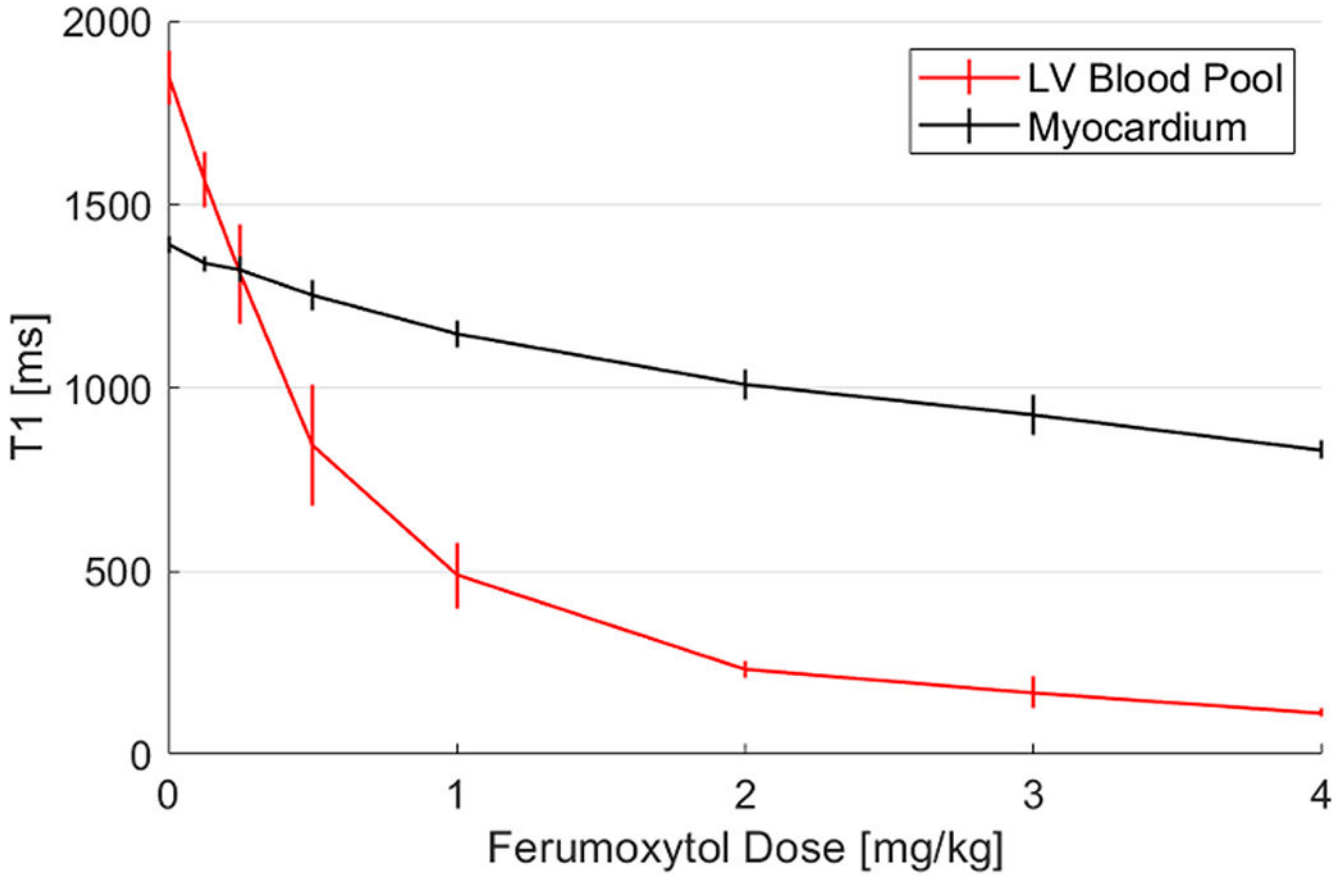

FIGURE 3.

Ferumoxytol dose-response curves for left ventricular (LV) blood pool and myocardial T1. T1 (ms) is plotted as mean ± sd. The multi-dose T1 imaging study captures the inversion of contrast between the myocardium and LV blood pool at approximately 0.25 mg/kg of ferumoxytol. This enables estimation of myocardial extravascular T1 ($T1_{ev}$) directly from myocardial T1 maps.

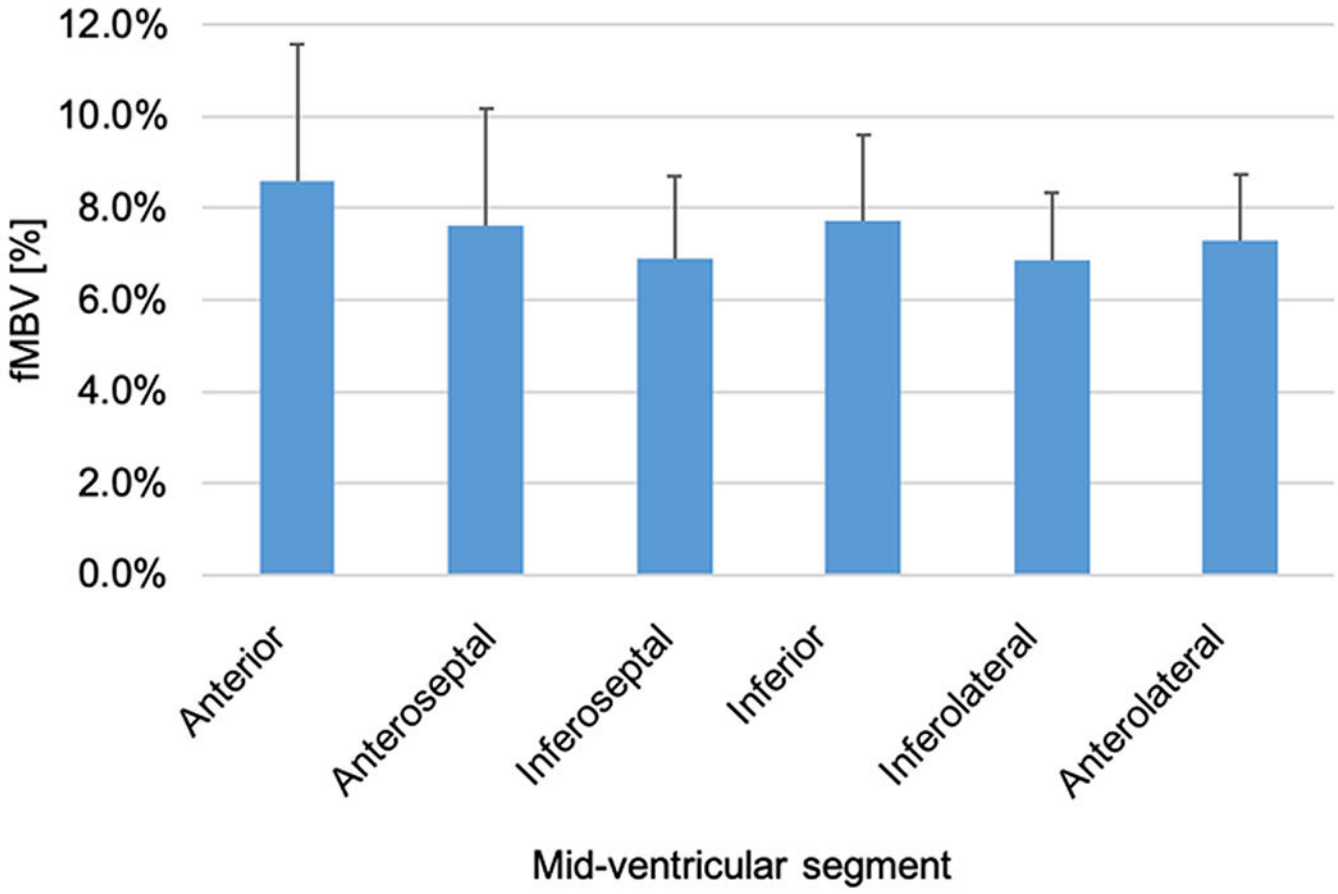

FIGURE 4.

Segmental fMBV in nine healthy swine models (mean ± SD). Mid-ventricular ferumoxytol multi-dose T1 images were contoured according to the AHA model (7, anterior; 8, anteroseptum; 9, inferoseptum; 10, inferior; 11, inferolateral; 12, anterolateral). fMBV was estimated using a two-compartment model with image-derived extravascular T1. One-way ANOVA shows significant variance in baseline fMBV between swine subjects (p=0.027), and no significant variance in fMBV between segments (p=0.387).

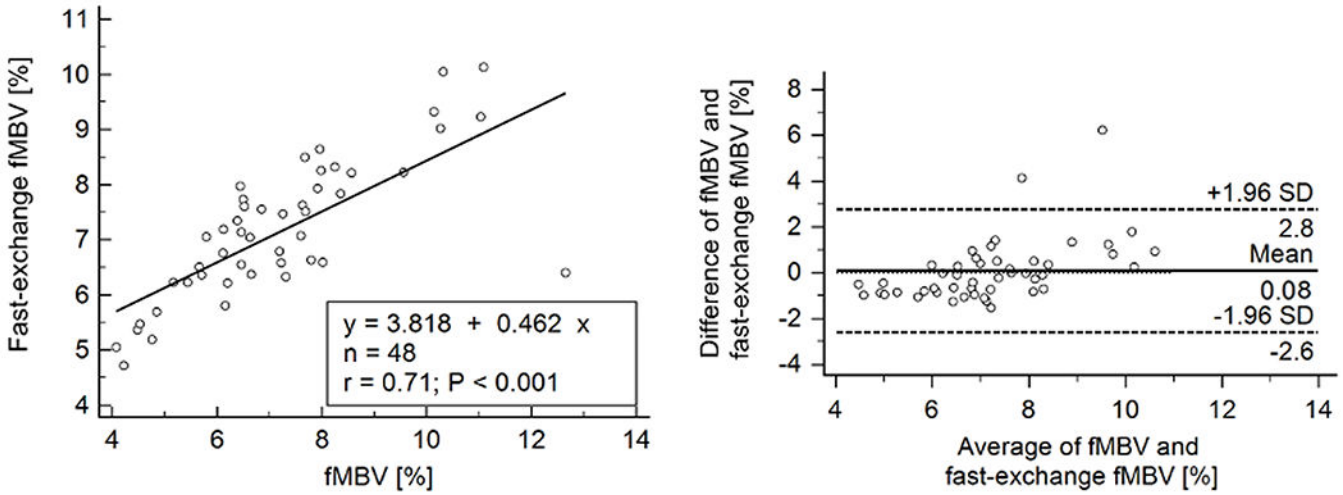

FIGURE 5.

Bland-Altman analysis of model-fitted and simple fast-exchange fMBV at 2.0 mg/kg ferumoxytol. The mean difference is 0.08 (p=0.688). Wide limits of agreement may obscure subtle findings in the clinical setting if a simple fast-exchange (equation 1–2) fMBV approach is used.

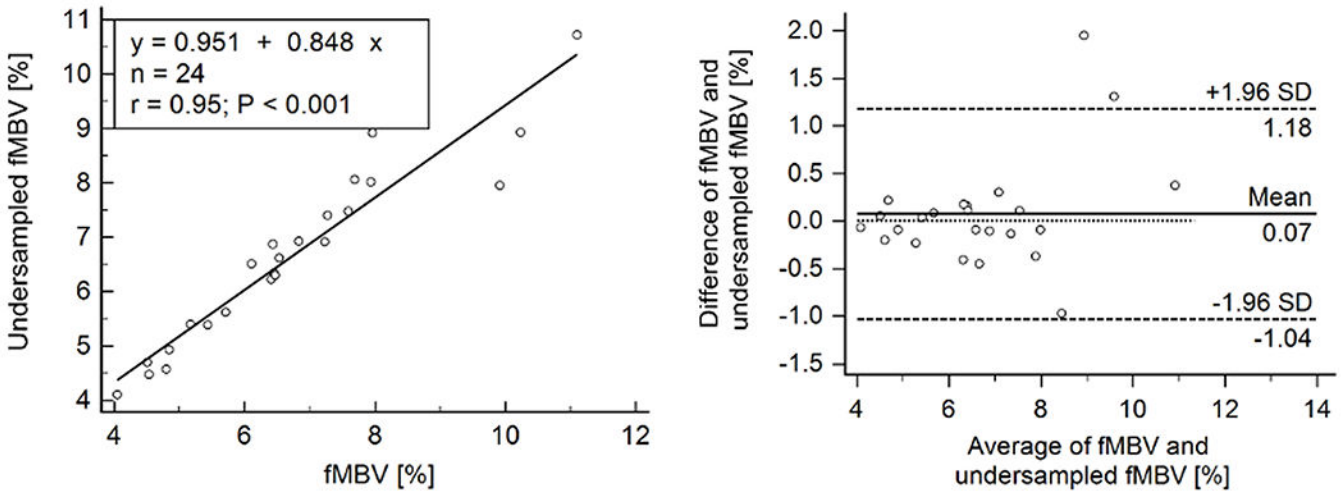

FIGURE 6.

Bland-Altman analysis of fMBV in 4 swine subjects fitted using the complete dataset and an undersampled dataset of 4 ferumoxytol doses (0.0, 0.125, 2.0, 4.0 mg/kg). The mean difference is 0.07 (p=0.541). Quantification of tissue perfusion using four T1 images during ferumoxytol infusion may be feasible.

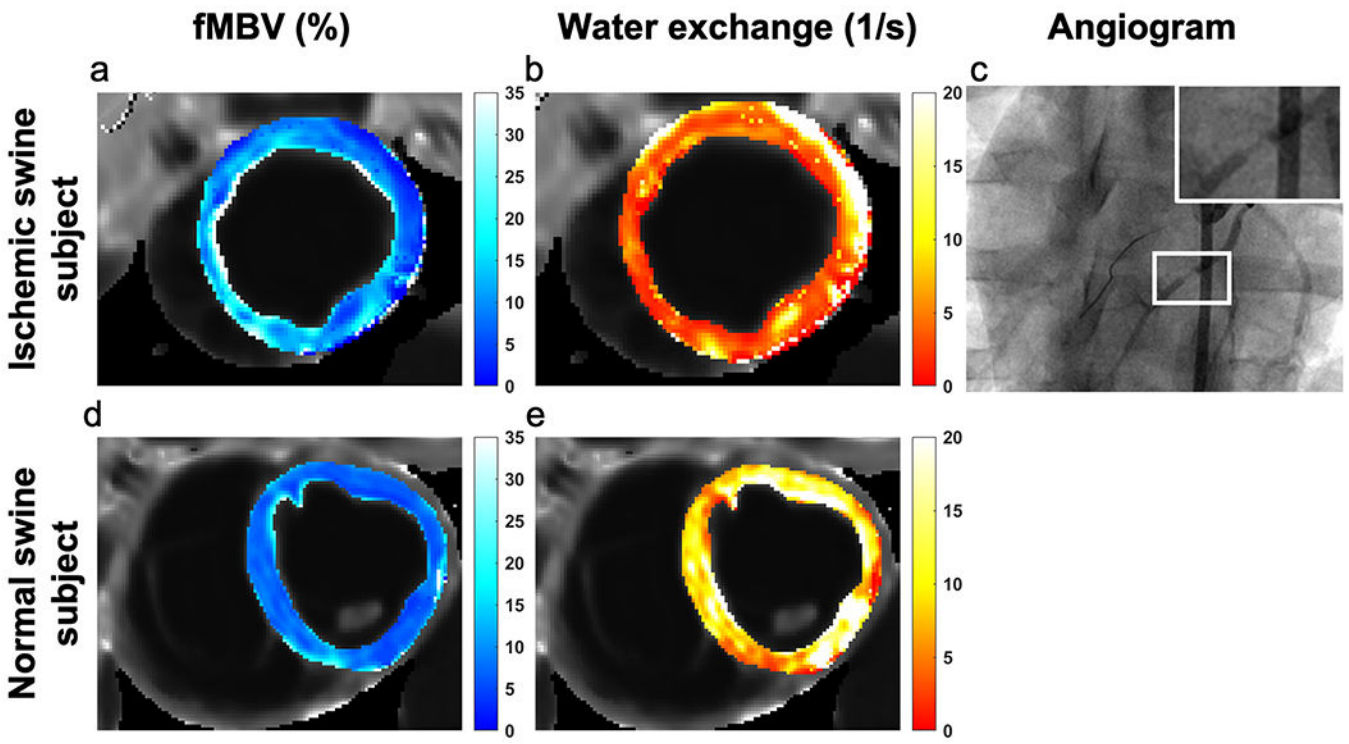

FIGURE 7.

Illustrative examples of pixelwise fMBV and water exchange maps in a swine model of regional myocardial hypoperfusion (a, b) and a normal swine subject (d, e). In the swine subject with artificially-induced coronary stenosis (top panel, a), we expect all myocardial segments downstream from the mid left anterior descending (LAD) coronary stenosis to be hypoperfused. Visual and quantitative differences in fMBV can be observed in the anterior, septal, and inferior segments that are hypoperfused by the stenotic LAD. Relative to the normal swine, water exchange is restricted in the hypoperfused segments of the swine with coronary stenosis. Angiographic image (c) acquired following deployment of a 3D-printed coronary implant in the mid LAD shows severe coronary narrowing.

Table 1.

Comparison of steady-state contrast-enhanced multi-compartmental models of myocardial blood volume and water exchange using iron-based contrast agents. fMBV and k_i reproduced as reported or computed from reported model parameters and results.

Study	Subject	Contrast	T1 sequence	Field strength	Model	fMBV (%)	k_i (s^{-1})
Wacker et al. (2002) (35)	Human, CAD (6)	NC100150	Saturation-recovery turboFLASH	1.5 T	2-compartment, model-fitted	12.9 *	3.72
Bjornerud et al. (2003) (19)	Swine, Healthy (8)	NC100150	Look-Locker	1.5 T	2-compartment, model-fitted	12.4±2.3	9.35±5.5
Bane et al. (2015) (17)	Canine, Healthy (1)	Ferumoxytol	5(3)3(3)3 MOLLI	1.5 T	2-compartment, slow exchange	5	14
Colbert et al.	Swine, Healthy (9)	Ferumoxytol	5(3)3(3)3 MOLLI	3.0 T	2-compartment, model-fitted	7.2 ± 1.4	11.3±5.1

*Wacker et al. report fMBV, water exchange fitted to complete (N=6) dataset. fMBV, fractional myocardial blood volume; k_i, intravascular water exchange rate.

Table 2.

Pixel-wise fMBV values in a swine model of myocardial hypoperfusion and a normal swine subject. Pixel-wise fMBV in each AHA segment reported as mean ± SD. Following image registration and fMBV fitting, left ventricular pixel-wise fMBV maps were contoured according to the AHA model.

Swine subject with myocardial hypoperfusion		
Myocardial Segment	**fMBV (%)**	**Water exchange rate (1/s)**
13 (apical anterior) *	11.90 ± 4.00	4.54 ± 1.89
14 (apical septum) *	16.10 ± 5.71	3.57 ± 2.11
15 (apical inferior)	9.59 ± 3.35	5.55 ± 3.68
16 (apical lateral)	8.38 ± 2.35	5.53 ± 2.90
Normal swine subject		
Myocardial Segment	fMBV (%)	Water exchange rate (1/s)
7 (mid anterior)	7.74 ± 1.70	11.29 ± 4.18
8 (mid anteroseptal)	8.36 ± 2.86	9.75 ± 3.85
9 (mid inferoseptal	7.83 ± 1.17	10.16 ± 3.95
10 (mid inferior)	8.13 ± 2.51	10.17 ± 5.38
11 (mid inferolateral)	7.33 ± 2.06	18.30 ± 12.90
12 (mid anterolateral)	7.10 ± 1.16	11.78 ± 3.35

* Segments perfused by the artificially-induced left anterior descending artery coronary stenosis.